Evaluation of the Accuracy of Real-time Digital Simulator Voltage Source Converter Models Determined from Frequency Scanning

Yi Qi, Aniruddha Gole, Hui Ding, Yi Zhang

***Abstract* — Two types of modeling method for the Voltage Source Converters (VSC) are typically used in a real time digital simulator (rtds). One uses the 'ON' and 'OFF' resistance to represent the different switching states (called as the 'R' model). The other, referred to as the 'LC' model, is more recent and faster, however makes approximations as it models the 'ON' switch as a small inductor and the 'OFF' switch as a small capacitor in series with a resistor. Hence, the accuracy of the 'LC' model is sometimes questioned, with the suspicion that the L and C elements may result in an unacceptably large error in the frequency response characteristics. To validate the accuracy of the 'LC' type model, the state space representation of the converter is developed to get the analytical approximation of frequency impedance. Then a frequency scan is conducted on the 'LC' type as well as the 'R' type converter via an rtds based EMT simulation to obtain the frequency impedance. The comparison between these three results proves that with properly selected parameters for the L and C components, the LC model is highly accurate.**

***Keywords*: VSC converter, rtds, 'R' approach, 'LC' approach, State space model, Frequency scanning.**

I. Introduction

The traditional model of VSC converter in many Electromagnetic Transient (EMT) simulators employs the different 'ON' and 'OFF' resistance values to simulate the different switching states of the semiconductors [1]. In this approach, the IGBT/diode switches as in Fig. 1.a, are represented by a small resistance R_{on} for the 'ON' state and a large resistance R_{off} for the 'OFF' state as in Fig. 1.b. However, with this approach, the admittance matrix in EMT simulation changes and needs to be re-factorized after a switching action. As long as the switching frequency is high, such as the case of two level VSC converter with Pulse Width Modulation (PWM), this high frequency and time-costly calculation makes the real time implementation a challenge.

An alternative 'LC' approach was developed [1-2], which uses a small inductor L_s ('L' branch) to represent the 'ON' state and a small capacitor C_s in series with a resistor R_s ('RC' branch) for the 'OFF' state, as in Fig. 1.c. Also, the converter is simulated with a much smaller simulation time step Δt_s as compared to the external ac system which has a larger time step Δt_b. The parameters of the 'LC' model are selected as in (1).

$$\frac{2L_s}{\Delta t_s} = \frac{\Delta t_s}{2C_s} + R_s \tag{1}$$

The $2L_s/\Delta t_s$ and $\Delta t_s/2C_s$ are the companion circuit equivalent impedance of the inductor and capacitor in EMT simulation. The inclusion of R_s minimizes the potential damping between the 'L' and 'RC' branch. With equation (1), it is guaranteed that the circuit impedances of the 'L' and 'RC' branch are the same, so that the switching from the 'ON' to 'OFF' state does not change the network impedance matrix. This eliminates the need for impedance matrix re-factorization on switching; only the formula to calculate history terms changes. Hence, the simulation time for each time step is reduced, allowing a smaller time step and better accuracy in real time simulation. When it comes to fundamental frequency (60Hz), the impedance of the 'OFF' state (the 'RC' branch) is much bigger than the 'ON' state (the 'RC' branch).

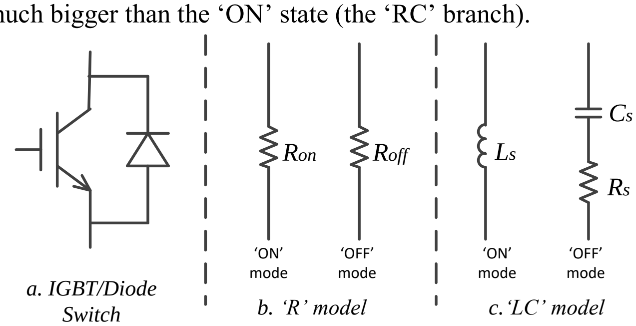

Figure. 1. Two types of IGBT models

Typical L_s and C_s are selected to be small numbers, for the case studied in below sections, these values are shown in Table I.

TABLE I
TYPICAL RLC VALUES IN 'LC' MODEL

Component	R_s	C_s	L_s
Values	*132ohm*	*0.017uF*	*0.15mH*

However, although the 'LC' approach is highly efficient numerically, there is a concern that replacing the 'ON' and 'OFF' resistances with inductances and capacitances, may excite spurious resonances.

This paper investigates this issue by conducting a frequency scan on a system containing a VSC converter modelled with the 'R' and the 'LC' approaches using an rtds simulator from RTDS Technologies. From this scanning, the

---

This work was supported in part by the NSERC and RTDS Technologies.
Yi Qi and Aniruddha Gole are with Department of Electrical and Computer Engineering, University of Manitoba, Winnipeg, Manitoba, Canada (email: qiy3@myumanitoba.ca).
Hui Ding and Yi Zhang are with RTDS Technologies, Winnipeg, Manitoba, Canada (email: hui@myumanitoba.ca).

Paper submitted to the International Conference on Power Systems Transients (IPST2017) in Seoul, Republic of Korea June 26-29, 2017

frequency impedance is extracted to reflect the converter characteristics shown to the network. At the same time, an analytical expression for the frequency response is derived from a small-signal state space model [3-5] of the converter as an approximate. The result comparison between the 'R' and 'LC' type converters proves that the 'LC' type model is highly accurate.

II. TEST SYSTEM

An example VSC converter with a simple ac and dc side system is constructed in rtds as shown in Fig. 2. The converter is modelled either using the fast 'LC' approach or the slower and more conventional 'R' approach.

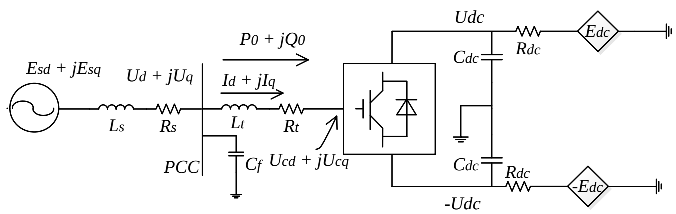

Figure. 2. Electrical system

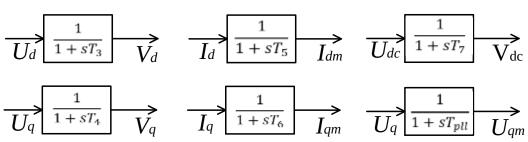

a. Measurement filter and per unit processing

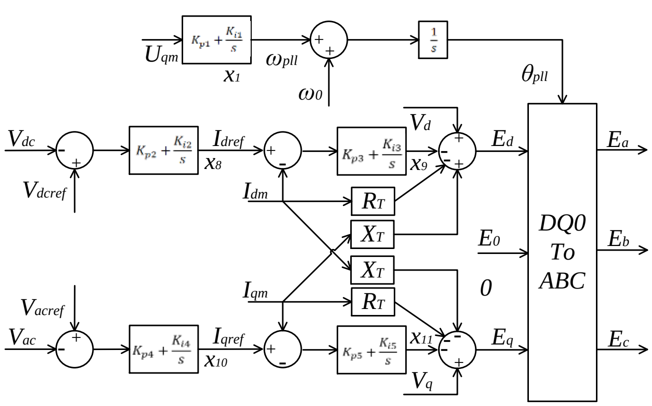

b. Decoupling control logic

Figure. 3. Control system of Converter

Fig. 3 shows the converter control system including a decoupled controller for the direct (d) and quadrature (q) currents, and a Phase Locked Loop (PLL) to synchronize the controller to the ac voltage. The system data is provided in the Appendix. A.

III. ANALYTICAL MODEL

The analytical model is developed to get an independent analytical frequency response of the converter's impedance. This is later compared with a scanning response obtained from simulation. The state space model is different from earlier research as it explicitly includes the R_{on} and R_{off} resistances, which could have a bearing on the damping performance.

A. Static frame reference

In this work, a static network d-q frame [4] rotating at source fundamental frequency ω_0 is chosen as the reference. The phase locked loop is used to track the ac voltage. The relative position between the PLL and static frame is shown in Fig. 4.

We choose the angle difference θ to have a nominal steady state value of 0 in this paper, which is convenient for calculation and comparison. The transformation of elements between the two frames (superscript 's' for static frame, 'p' for PLL frame) is:

$$\begin{bmatrix} X_d{}^s \\ X_q{}^s \end{bmatrix} = \begin{bmatrix} cos\theta & -sin\theta \\ sin\theta & cos\theta \end{bmatrix} \begin{bmatrix} X_d{}^p \\ X_q{}^p \end{bmatrix} \quad (2)$$

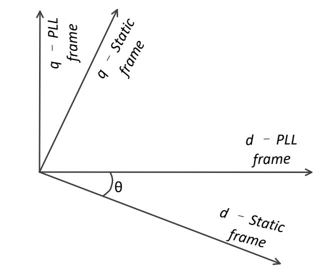

Figure. 4. Position of PLL and static frame

Linearization gives:

$$\begin{bmatrix} \Delta X_d{}^s \\ \Delta X_q{}^s \end{bmatrix} = \begin{bmatrix} cos\theta & -sin\theta \\ sin\theta & cos\theta \end{bmatrix} \begin{bmatrix} \Delta X_d{}^p \\ \Delta X_q{}^p \end{bmatrix} + \begin{bmatrix} -sin\theta & -cos\theta \\ cos\theta & -sin\theta \end{bmatrix} \begin{bmatrix} X_d{}^p \\ X_q{}^p \end{bmatrix} \Delta\theta \quad (3)$$

B. Influence of 'ON' and 'OFF' resistance

The previous works [3-5] take the 'ON' resistance as 0 and 'OFF' resistance as infinite in analytical modeling. Here actual switch resistance values can be included to get a better result of the damping.

The switch states for each of the R's in the 'a' phase leg of a three-phase converter is shown in Fig. 5. The resistances alternately take on values of R_{on} and R_{off} as decided by two complementary PWM modulated waveforms. The resulting ac side waveform has the same shape as the upper PWM signal and alternatively switches between $+U_{dc}$ and $-U_{dc}$, where U_{dc} is the dc capacitor voltage.

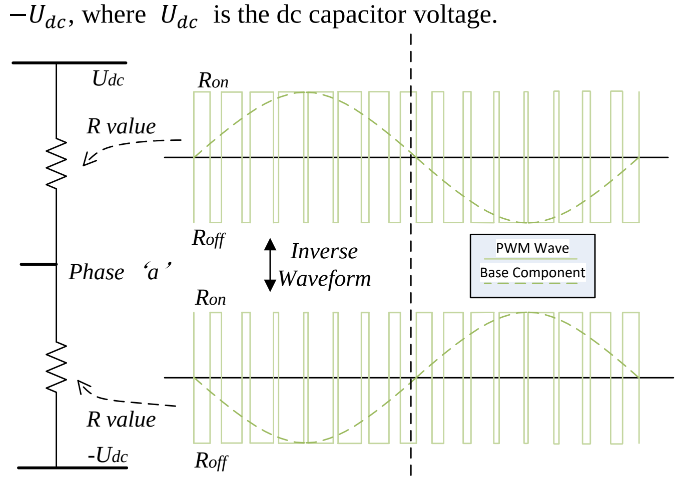

Figure. 5. PWM switching states for the switches

Based on Fig 5, we obtain the equivalent circuit for the converter as in Fig. 6. The ac side network is connected through the 'R_{on}' to the modulated waveform of dc voltage $\left(E_d{}^s + jE_q{}^s\right) * U_{dc}$ ($E_d{}^s$ and $E_q{}^s$ are the outputs of the control system coming from (29)), and through the 'R_{off}' to the inversed modulated waveform equal to $-\left(E_d{}^s + jE_q{}^s\right) * U_{dc}$. The positive dc side is connected to two current sources, which are the products of two ac current values (from Fig 6.a) and the PWM switching function, and the negative dc side is symmetrical to the positive side.

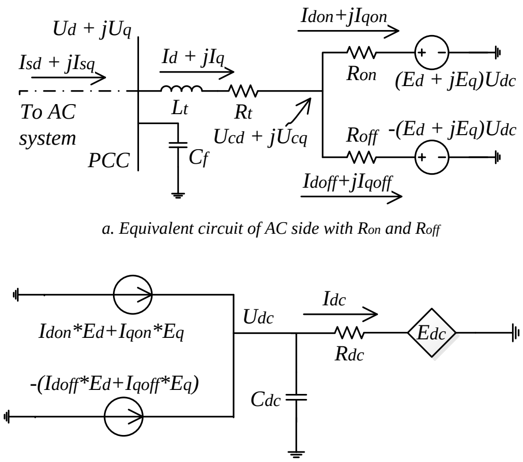

a. Equivalent circuit of AC side with R_{on} and R_{off}

b. Equivalent circuit of DC positive side with R_{on} and R_{off}

Figure. 6. Equivalent circuit of ac and dc side with R_{on} and R_{off}

We can write the analytical equations for Fig. 6.a:

$$C_f \frac{d}{dt}\begin{bmatrix} U_d{}^s \\ U_q{}^s \end{bmatrix} + \begin{bmatrix} 0 & -\omega_0 C_f \\ \omega_0 C_f & 0 \end{bmatrix}\begin{bmatrix} U_d{}^s \\ U_q{}^s \end{bmatrix} = \begin{bmatrix} I_{sd}{}^s \\ I_{sq}{}^s \end{bmatrix} - \begin{bmatrix} I_d{}^s \\ I_q{}^s \end{bmatrix} \quad (4)$$

$$L_t \frac{d}{dt}\begin{bmatrix} I_d{}^s \\ I_q{}^s \end{bmatrix} + \begin{bmatrix} R_t + R_c & -\omega_0 L_t \\ \omega_0 L_t & R_t + R_c \end{bmatrix}\begin{bmatrix} I_d{}^s \\ I_q{}^s \end{bmatrix} = \begin{bmatrix} U_d{}^s \\ U_q{}^s \end{bmatrix} - \begin{bmatrix} E_d{}^s \\ E_q{}^s \end{bmatrix} U_{dc} * k \quad (5)$$

$$\begin{bmatrix} I_{don}{}^s \\ I_{qon}{}^s \end{bmatrix} = \frac{-2\begin{bmatrix} E_d{}^s \\ E_q{}^s \end{bmatrix} U_{dc} + R_{off}\begin{bmatrix} I_d{}^s \\ I_q{}^s \end{bmatrix}}{R_{off} + R_{on}} \quad (6)$$

$$\begin{bmatrix} I_{doff}{}^s \\ I_{qoff}{}^s \end{bmatrix} = \frac{2\begin{bmatrix} E_d{}^s \\ E_q{}^s \end{bmatrix} U_{dc} + R_{on}\begin{bmatrix} I_d{}^s \\ I_q{}^s \end{bmatrix}}{R_{off} + R_{on}} \quad (7)$$

Superscript 's' indicates the static frame; $E_d{}^s$ and $E_q{}^s$, coming from (27), are the outputs of the control system. In (5), the k and R_c values are:

$$k = (R_{off} - R_{on})/(R_{off} + R_{on}),\ R_c = R_{off}||R_{on}.$$

The analytical equations for Fig. 6.b:

$$C_{dc}\frac{dU_{dc}}{dt} = \left(\begin{bmatrix} I_{don}{}^s \\ I_{qon}{}^s \end{bmatrix} - \begin{bmatrix} I_{doff}{}^s \\ I_{qoff}{}^s \end{bmatrix}\right)^T \begin{bmatrix} E_d{}^s \\ E_q{}^s \end{bmatrix} - I_{dc} \quad (8)$$

C. State space model

The state space model is obtained by linearizing the equations: (2-8), and (14-29). It is easy to get the form:

$$\begin{cases} \Delta\dot{X} = A\Delta X + B\Delta U \\ \Delta Y = C\Delta X + D\Delta U \end{cases} \quad (9)$$

With this state space model the frequency impedance could be conducted. However, it has to be specified that the analytical model is an approximate as it uses an averaged switching function to represent the transformation between ac and dc sides of the converter. Thereby, the main purpose of this part is not as an accurate template for comparison, but as a sanity check to the experimental results.

IV. Frequency Scanning

The frequency scanning method [6] [7] was introduced to study the small signal harmonic impedance of a Line Commutated Converter (LCC). As the EMT model of the LCC system is constructed, a harmonic current (or voltage), containing several equi-magnitude frequency components as given by (10) is injected at the node at which the impedance of the system is desired. The injected components have a very small magnitude X_{mag}, so as not to affect the operating point of the system. In order to prevent bunching in the time domain waveform, a non-linear phase shift is added to each sinusoidal component [6]. The corresponding voltage (or current) is measured and its harmonic components extracted using the Discrete Fourier Transform (DFT). Dividing the resultant voltage (current) component by X_{mag} gives the impedance (admittance) at each frequency.

$$\mathrm{X}_{inj}(t) = \sum_{f=fmin}^{fmax} X_{mag}\cos\left(2\pi f t + k_{inj} f^2\right) \quad (10)$$

The scanning can be done in the d-q domain or phase (abc) domain as discussed later.

A. Impedance looking from ac and dc sides

The impedances looking from the ac and dc side are both measured by suitable injections as shown in Fig. 7.

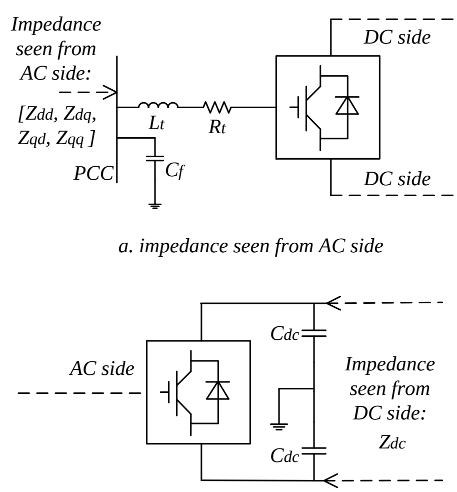

a. impedance seen from AC side

b. impedance seen from in AC side

Figure. 7. Impedance to be scanned from ac and dc side

For the ac side, as shown in Fig. 7.a. the impedance is measured from the Point of Common Coupling (PCC) bus. Hence, the impedance scan includes the ac capacitor branch and the reflected impedance of the dc side as seen through the converter's ac side. The small signal virtual current injection to the ac capacitor and converter branch is set as input of the system, and the small signal voltage output in PCC bus is set as output.

As in Fig. 7.b, for the dc side, the impedance measurement includes the dc capacitor bus, in parallel with the reflected impedance of the ac side viewed through the converter's dc terminals.

B. Injection signals

In practical scanning, one can use either current or voltage injection. As specified in [8] [9], the perturbation injection location need not be at the location where the impedance or admittance needs to be measured. In that case, one simply divides the DFT components of the voltage (current) and current (voltage) at the location of interest to get the impedance (admittance). In this paper, for convenience, we choose to inject a voltage.

C. d-q-0 domain

It can be shown that if phase coordinates are used to obtain a frequency response, there can be coupling in the frequencies. For example, if a positive sequence current of frequency ω is injected into the converter at its ac bus, measured voltages on the bus will include a positive sequence component at frequency ω, as well as a negative sequence component at frequency ω - 2ω₀, where ω₀ is the fundamental frequency [10]. However, if the circuit is represented in d-q-0 coordinates, the coupling between frequencies disappears [3]. But a coupling can still exist between the d and q quantities. Equation (11) is used to transform between phase a-b-c and d-q-0 coordinates.

$$\begin{cases} \begin{bmatrix} X_d \\ X_q \\ X_0 \end{bmatrix} = \frac{2}{3}\begin{bmatrix} cos\theta_t & \cos(\theta_t - \frac{2}{3}\pi) & \cos(\theta_t + \frac{2}{3}\pi) \\ -sin\theta_t & -sin(\theta_t - \frac{2}{3}\pi) & -\sin(\theta_t + \frac{2}{3}\pi) \\ 1/2 & 1/2 & 1/2 \end{bmatrix} \begin{bmatrix} X_a \\ X_b \\ X_c \end{bmatrix} \\ \begin{bmatrix} X_a \\ X_b \\ X_c \end{bmatrix} = \begin{bmatrix} cos\theta_t & -sin\theta_t & 1 \\ \cos(\theta_t - \frac{2}{3}\pi) & -sin(\theta_t - \frac{2}{3}\pi) & 1 \\ \cos(\theta_t + \frac{2}{3}\pi) & -sin(\theta_t + \frac{2}{3}\pi) & 1 \end{bmatrix} \begin{bmatrix} X_d \\ X_q \\ X_0 \end{bmatrix} \end{cases} \quad (11)$$

Where the reference angle $\theta_t = \omega_0 t + \theta_0$. The $\omega_0 t$ is for static rotating frame, and the offset angle θ_0 is used to ensure that $U_q = 0$. There is no zero-sequence current flow path, we have $I_0 = 0$. Hence, the scanning in this paper does inject only d and q direction currents. To do this, the d and q axis voltage injections are selected in the form (10), and then the phase injections $(v_a,\ v_b,\ v_c)$ are calculated using (11) and injected into the network in the simulation. Again, a d-q-0 transformation is applied to the measured phase currents to get d-q components and then the frequency components are obtained using a DFT. Once we have the frequency components of current and voltage, the admittance or impedance is readily calculated by division.

The ac side impedance under d-q domain is a 2*2 dim matrix:

$$Z_{ac}(\omega) = \begin{bmatrix} Z_{dd}(\omega) & Z_{dq}(\omega) \\ Z_{qd}(\omega) & Z_{qq}(\omega) \end{bmatrix} \quad (12)$$

To obtain the four impedances in (12), we first inject voltage and observe the resultant d and q direction currents $(i_{d\_1}(\omega),\ i_{q\_1}(\omega))$ and voltages $(v_{d\_1}(\omega),\ v_{q\_1}(\omega))$. We then inject a different ratio of d-q direction currents, then the resultant current $(i_{d\_2}(\omega),\ i_{q\_2}(\omega))$ and voltage $(v_{d\_2}(\omega),\ v_{q\_2}(\omega))$ is measured. The impedances can then be obtained from (13).

$$\begin{bmatrix} Z_{dd}(\omega) & Z_{dq}(\omega) \\ Z_{qd}(\omega) & Z_{qq}(\omega) \end{bmatrix} = \begin{bmatrix} v_{d\_1}(\omega) & v_{d\_2}(\omega) \\ v_{q\_1}(\omega) & v_{q\_2(\omega)} \end{bmatrix} * \begin{bmatrix} i_{d\_1}(\omega) & i_{d\_2}(\omega) \\ i_{q\_1}(\omega) & i_{q\_2}(\omega) \end{bmatrix}^{-1} \quad (13)$$

D. Measuring

The sampling time step and sampling window of voltage and current depends on the frequencies injected. The sampling window should always bigger than a cycle of any frequency in the injecting series. When the system contains some high frequency harmonics as the background noise, a low pass digital filter is used to pre-process the sampled data.

V. Result of Frequency Impedance

A. System settings

The frequency scanning is employed on both the 'R' approach and the 'LC' approach converter in rtds. In the 'R' approach converter, the 'ON' and 'OFF' resistance values are: $R_{on} = 0.002PU$, and $R_{off} = 2000PU$. These values are also applied in the analytical model.

The simulations are conducted with a time step of 50 µs for the external network and 500 ns for the converter model. Considering that the frequency characteristic of the impedance for the VSC converter (no matter looking from ac or dc side) depends on the operating point, two typical operating points are chosen in this paper for comparison, as in Table II, with different active and reactive powers from the PCC bus to the converter, as shown in Fig. 2.

TABLE II
OPERATING POINTS

Operating point	P_0	Q_0
1	*1 PU*	*0 PU*
2	*0.6 PU*	*0.2 PU*

B. Impedance comparison in operating point 1

At operating point *1*, the VSC is operating at maximum active power. The comparison of ac and dc impedance scans for the 'R' model, the 'LC' model and the analytical results is shown in Figs. 8 to 10, in the frequency range 1 Hz to 1000 Hz, which is enough for most of the network stability studies.

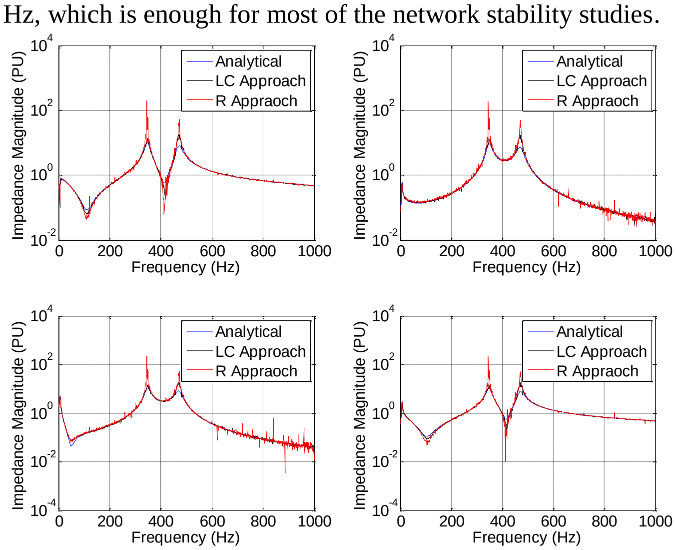

Figure. 8. Ac side impedance magnitude (Zdd Zdq Zqd Zqq)

In Fig. 8 to 9, the four subplots are the d-q domain coupled impedances looking from the ac side: Z_{dd}, Z_{dq}, Z_{qd} and Z_{qq}(see Fig. 7.a).

Fig. 8 shows the magnitude responses (in per unit) and Fig. 9 shows the phase angles (in degrees). Fig. 10 shows the magnitude (in per unit) phase angle (in degrees) of the impedance looking from the dc side: Z_{dc} (see Fig. 7.b). From these curves, it is easily found, the scanned results and the analytical result match very well.

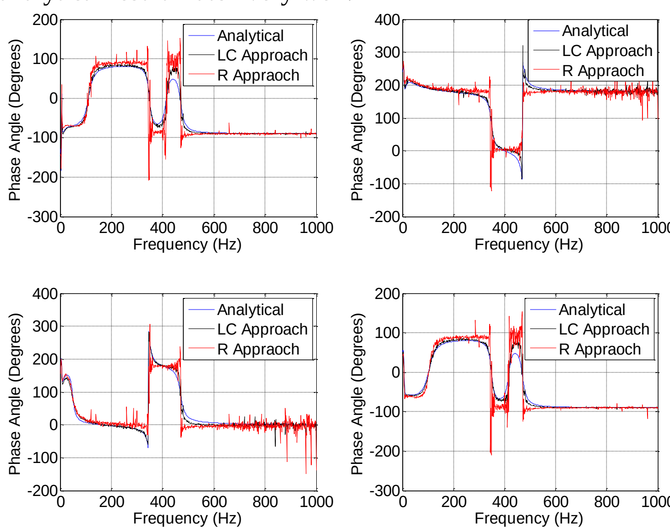

Figure. 9. Ac side impedance phase angle (Zdd Zdq Zqd Zqq)

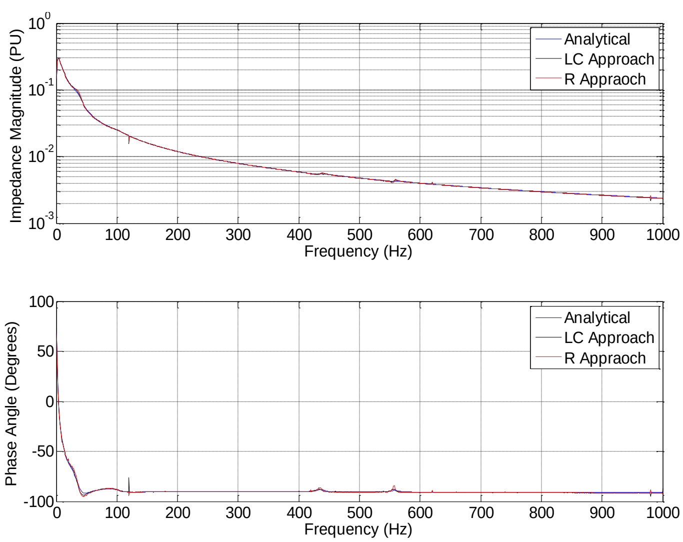

Figure. 10. Dc side impedance magnitude and phase angle

C. Impedance comparison in operating point II

Fig. 11-12 are the magnitude and phase angle of impedance looking from the ac side and Fig. 13 shows the result looking from the dc side. This impedance response is also obtained from a simulation with 50 μs large time step for external network (2 μs for converter network) in rtds.

In this operating point, the impedance results also match very well, which means the 'LC' approach model is also reliable at this operating point.

At the same time we could also make the same comparison step for the frequency response under other operating points, it is not listed in this paper due to the page restriction.

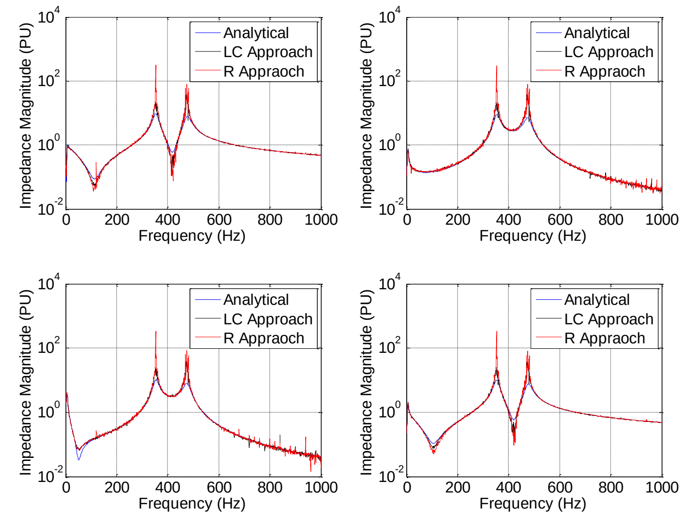

Figure. 11. Ac side impedance magnitude (Zdd Zdq Zqd Zqq)

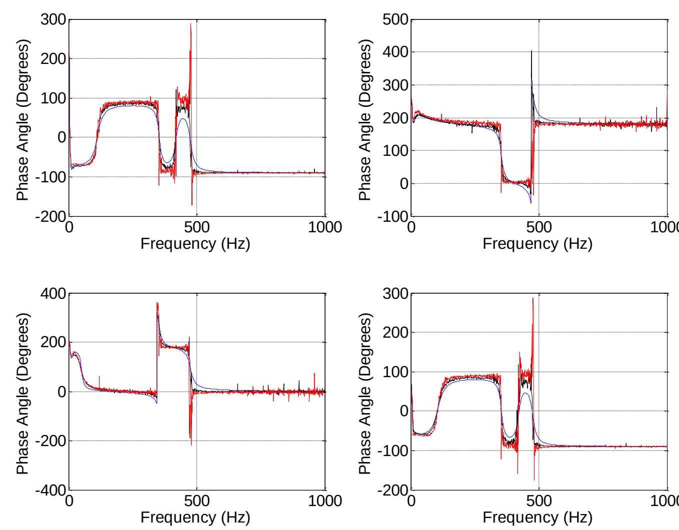

Figure. 12. Ac side impedance phase angle (Zdd Zdq Zqd Zqq)

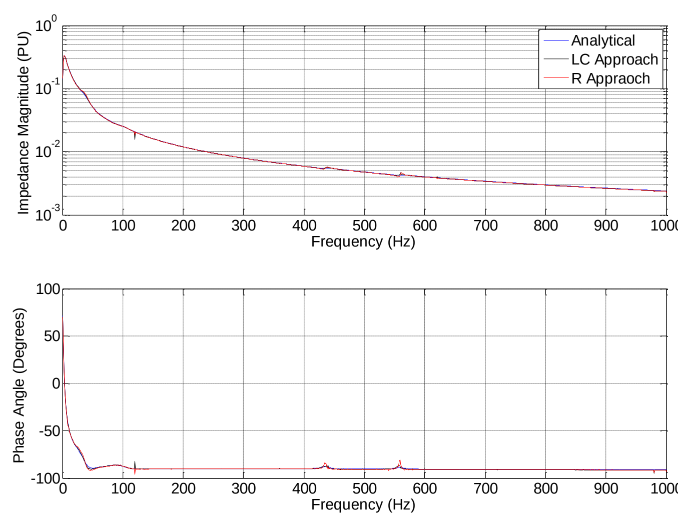

Figure. 7. Dc side impedance magnitude and phase angle

VI. CONCLUSIONS AND DISCUSSIONS

This work investigates the impedance characteristic of the converter model in rtds (both 'R' and 'LC' approach types), with a view to validating the 'LC' model. Using detailed EMT simulation on the rtds of a VSC-HVDC converter with realistic controls, experimental frequency scans are conducted on the 'R' and 'LC' models with the converter operating at two different operating points. The comparison between these two impedance results, as well as the analytical result, shows that the 'LC' model has very good accuracy, making it a good choice for real-time simulation.

In this paper, we are mainly discussing on the specific 'LC' type 2-level VSC model on the rtds platform. Moreover, for the recently developed Modular Multilevel Converter (MMC), as long as the internal details are ignored, for the averaged value models using the same switching functions, much of the external behavior is probably still predictable using the result of this paper [11].

VII. APPENDIX

A. System and Controller Data

The electrical system parameters in Fig. 2 are as follows:

TABLE III
CIRCUIT DATA OF ELECTRICAL SYSTEM

Parameters	Value	Parameters	Value
Ac base voltage (L-L RMS)	100kV	L_s	0.026526H
Dc base voltage	100kV	R_t	1ohm
System base Mva	300MVA	L_t	0.013263H
C_f	11.937μF	C_{dc}	1000μF
R_s	2ohm		

The dc side resistance R_{dc} is subject to the operating point and we choose a pure resistive load for dc side (E_{dc} is 0 if no voltage injection). Then the impedance characteristic would not be significantly affected by this resistance (a small resistance would short circuit the dc capacitor).

For the control system in Fig. 3, the parameters are:

TABLE IV
CONTROL SYSTEM DATA

Parameters	Value	Parameters	Value
T_3	0.02	K_{p3}	1
T_4	0.02	K_{p4}	2
T_5	0.004	K_{p5}	1
T_6	0.004	K_{i1}	33.3
T_7	0.005	K_{i2}	50
T_{pll}	0.005	K_{i3}	10
K_{p1}	20	K_{i4}	50
K_{p2}	2	K_{i5}	10

B. Analytical Model

The differential equations for the analytical model for the system beside the converter part are shown below (superscript 's' for static frame, 'p' for PLL frame). For the ac system R-L branch, the equation:

$$L_s \frac{d}{dt}\begin{bmatrix} I_{sd}{}^{s} \\ I_{sq}{}^{s} \end{bmatrix} + \begin{bmatrix} R_s & -\omega_0 L_s \\ \omega_0 L_s & R_s \end{bmatrix}\begin{bmatrix} I_{sd}{}^{s} \\ I_{sq}{}^{s} \end{bmatrix} = \begin{bmatrix} E_{sd}{}^{s} \\ E_{sq}{}^{s} \end{bmatrix} - \begin{bmatrix} U_d{}^{s} \\ U_q{}^{s} \end{bmatrix} \quad (14)$$

The voltage and current measuring process, as well as the decoupling control system:

$$T_{vd}\dot{V}_{dc} = U_{dc} - V_{dc} \quad (15)$$

$$T_v \dot{V}_d = U_d{}^{p} - V_d \quad (16)$$

$$T_v \dot{V}_q = U_q{}^{p} - V_q \quad (17)$$

$$T_i \dot{I}_{dm} = I_d{}^{p} - I_{dm} \quad (18)$$

$$T_i \dot{I}_{qm} = I_q{}^{p} - I_{qm} \quad (19)$$

$$\dot{I}_{dref} = K_{i2}\left(V_{dcref} - V_{dc}\right) + K_{p2}\left(\dot{V}_{dcref} - \dot{V}_{dc}\right) \quad (20)$$

$$\dot{E}_d = \dot{V}_d + \omega_0 L_t \dot{I}_{qm} - R_t \dot{I}_{dm} - K_{i3}\left(I_{dref} - I_{dm}\right) - K_{p3}\left(\dot{I}_{dref} - \dot{I}_{dm}\right) \quad (21)$$

$$\dot{I}_{qref} = K_{i4}\left(V_{acref} - \sqrt{V_d{}^{2} + V_q{}^{2}}\right) + K_{p4}\left(\dot{V}_{acref} - \dot{\sqrt{V_d{}^{2} + V_q{}^{2}}}\right) \quad (22)$$

$$\dot{E}_q = \dot{V}_q - \omega_0 L_t \dot{I}_{dm} - R_t \dot{I}_{qm} - K_{i5}\left(I_{qref} - I_{qm}\right) - K_{p5}\left(\dot{I}_{qref} - \dot{I}_{qm}\right) \quad (23)$$

The PLL:

$$\begin{bmatrix} U_d{}^{p} \\ U_q{}^{p} \end{bmatrix} = \begin{bmatrix} cos\theta & sin\theta \\ -sin\theta & cos\theta \end{bmatrix}\begin{bmatrix} U_d{}^{s} \\ U_q{}^{s} \end{bmatrix} \quad (24)$$

$$T_{pll}\dot{U}_{qm} = U_q{}^{p} - U_{qm} \quad (25)$$

$$\dot{\omega} = K_{i1} U_{qm} + K_{p1}\dot{U}_{qm} \quad (26)$$

$$\dot{\theta} = \omega \quad (27)$$

The transformation from the output of control system to static frame:

$$\begin{bmatrix} E_d{}^{s} \\ E_q{}^{s} \end{bmatrix} = \begin{bmatrix} cos\theta & -sin\theta \\ sin\theta & cos\theta \end{bmatrix}\begin{bmatrix} E_d \\ E_q \end{bmatrix} \quad (28)$$

The dc side R branch (E_{dc} is 0):

$$I_{dc} = \frac{U_{dc}}{R_{dc}} \quad (29)$$

VIII. REFERENCES

[1] RTDS Technologies, Real time digital simulation for the power industry manual set, Winnipeg, Canada, 2006.

[2] Trevor Maguire and James Giesbrecht, "Small Time-step (<2uSec) VSC Model for the Real Time Digital Simulator", Proceeding of IPST 2005, Montreal Canada, June 2005, Paper No. IPST-168-25c.

[3] J. Z. Zhou, H. Ding, S. Fan, Y. Zhang and A. M. Gole, "Impact of Short-Circuit Ratio and Phase-Locked-Loop Parameters on the Small-Signal Behavior of a VSC-HVDC Converter," *IEEE Transactions on Power Delivery*, vol. 29, no. 5, pp. 2287-2296, Oct. 2014.

[4] L. Zhang, Modeling and control of VSC-HVDC links connected to weak ac systems, Ph.D. dissertation, School of Elect. Eng., Royal Institute of Technology, Stockholm, Sweden, 2009.

[5] S. Arunprasanth, U. D. Annakkage, C. Karawita and R. Kuffel, "Generalized Frequency-Domain Controller Tuning Procedure for VSC Systems," in *IEEE Transactions on Power Delivery*, vol. 31, no. 2, pp. 732-742, April 2016.

[6] Xiao Jiang and A. M. Gole, "A frequency scanning method for the identification of harmonic instabilities in HVDC systems," in *IEEE Transactions on Power Delivery*, vol. 10, no. 4, pp. 1875-1881, Oct 1995.

[7] I. Papic and A. M. Gole, "Frequency response characteristics of the unified power flow controller," in *IEEE Transactions on Power Delivery*, vol. 18, no. 4, pp. 1394-1402, Oct. 2003.

[8] G. Francis, R. Burgos, D. Boroyevich, F. Wang and K. Karimi, "An algorithm and implementation system for measuring impedance in the D-Q domain," *2011 IEEE Energy Conversion Congress and Exposition*, Phoenix, AZ, 2011, pp. 3221-3228.

[9] B. Wen, D. Boroyevich, P. Mattavelli, Z. Shen and R. Burgos, "Experimental verification of the Generalized Nyquist stability criterion for balanced three-phase ac systems in the presence of constant power loads," *2012 IEEE Energy Conversion Congress and Exposition (ECCE)*, Raleigh, NC, 2012, pp. 3926-3933.

[10] M. Mohaddes, A. M. Gole and S. Elez, "Steady state frequency response of STATCOM," in *IEEE Transactions on Power Delivery*, vol. 16, no. 1, pp. 18-23, Jan 2001.

[11] T. Li, A. M. Gole and C. Zhao, "Harmonic Instability in MMC-HVDC Converters Resulting From Internal Dynamics," in *IEEE Transactions on Power Delivery*, vol. 31, no. 4, pp. 1738-1747, Aug. 2016.